Neoplasia 61 (2025) 101131

Contents lists available at ScienceDirect

Neoplasia

journal homepage: www.elsevier.com/locate/neo

Original Research

YPEL2 regulates the efficacy of BRD4-EZH2 dual targeting in EZH2^{Y641mut} germinal center-derived lymphoma

Aránzazu Chamorro-Jorganes [a,1], Núria Profitós-Pelejà [a,b,1], Clara Recasens-Zorzo [a], Juan G Valero [a,c], Diana Reyes-Garau [b], Laura Magnano [a], Ray Butler [d], Antonio Postigo [e], Patricia Pérez-Galán [a,c], Marcelo Lima Ribeiro [b,f,2], Gaël Roué [b,2,*]

[a] Division of Hemato-oncology, Institut d'Investigacions Biomèdiques August Pi i Sunyer (IDIBAPS), Barcelona, Spain
[b] Lymphoma Translational group, Josep Carreras Leukaemia Research Institute (IJC), Badalona, Spain
[c] Centro de Investigación Biomédica en Red-Oncología (CIBERONC), Madrid, Spain
[d] Butler Scientifics, Barcelona, Spain
[e] Group of Gene Regulation of Stem Cells and Cell Plasticity, IDIBAPS, ICREA, Barcelona, Spain
[f] Laboratory of Immunopharmacology and Molecular Biology, Sao Francisco University Medical School, Braganca Paulista, Sao Paulo, Brazil

ARTICLE INFO

Keywords:
Non-Hodgkin lymphoma
Epigenetics
Targeted therapies
Biomarkers
Mouse model

ABSTRACT

A significant proportion of diffuse large B cell lymphoma (DLBCL) and follicular lymphoma (FL) cases harbor a gain-of-function, heterozygous somatic mutation of the methyltransferase gene EZH2. While this factor is known to cooperate with the proto-oncogene MYC during malignant B cell development, the effect of interfering with both factors remains underexplored. Here we undertook the simultaneous evaluation of two epigenetic drugs targeting EZH2 methyltransferase activity and BRD4-mediated control of *MYC* transcription, CPI169 and CPI203, using preclinical models of DLBCL and FL with distinct EZH2 mutational status. We observed a specific and synergistic antiproliferative effect of these compounds in EZH2-mutated cells and mouse xenograft models, that was related to the abrogation of MYC transcriptional program and to tumor cell proliferation blockade at the G1 cell cycle phase. Gene expression profile, exploratory data analysis, and siRNA screening identified the PI3K/AKT-regulated gene and mitosis regulator, YPEL2, as a crucial factor involved in the efficacy of MYC/EZH2 dual targeting both *in vitro* and *in vivo*. Altogether, our results provide first pre-clinical evidence that simultaneous targeting of MYC and EZH2 is a safe and efficient approach that can be monitored by specific biomarkers, in aggressive lymphoid tumors of germinal center origin.

Introduction

Disruption of chromatin modulation is a key step in malignant hematopoiesis. Mutations in chromatin modifiers are common in hematological cancers and are often associated with aberrant cell fate decisions [1]. Genome-wide studies showed that these mutations are common events in B-cell non-Hodgkin lymphoma (B-NHL), with somatic mutations identified in several histone-modifying genes. Among the altered genes, a Y641 mutation affecting exon 15 of *the Enhancer of Zeste 2* (EZH2) gene occurs in 22 % of diffuse large B cell lymphoma (DLBCL) cases with germinal center B cell phenotype (GCB-DLBCL) and 27 % of follicular lymphoma (FL) cases, while it is absent in DLBCL with activated B cell phenotype (ABC-DLBCL) [2,3].

EZH2 encodes a histone methyltransferase, the catalytic subunit of Polycomb repressive complex 2, which silences genes by adding methyl groups to the lysine 27 residue of histone3 (H3K27). Heterozygous somatic point mutations in the EZH2 SET domain, primarily at the Y641 residue, enhance its enzymatic activity by converting mono- or dimethylated H3K27 to a trimethylated state, leading to the repression of target genes [2]. In germinal center (GC)-derived lymphomas like FL and GCB-DLBCL, where *EZH2* is highly expressed along with *BCL6*, the methyltransferase blocks DNA damage response pathways, allowing cell survival during somatic hypermutation of antibody maturation [4,5]. Additionally, *EZH2* mutations are linked to *BCL2* rearrangement in 28 %

* Corresponding author: Lymphoma Translational Group, Josep Carreras Leukaemia Research Institute, Badalona 08916, Spain.
E-mail address: groue@carrerasresearch.org (G. Roué).
[1] A. Chamorro-Jorganes and N. Profitós-Pelejà contributed equally to this work.
[2] M.L. Ribeiro and G. Roué share the senior authorship.

https://doi.org/10.1016/j.neo.2025.101131
Received 24 December 2024; Received in revised form 23 January 2025; Accepted 27 January 2025

of FL cases(and 33 % of GCB-DLBCL cases, and play a crucial role in MYC-associated lymphomagenesis in B cells [6–8]. EZH2 mutations and MYC overexpression cooperatively accelerate lymphomagenesis, as shown in Eμ-Myc/EZH2Y641F transgenic mice with faster lymphoma development and increased organ infiltration compared to Eμ-Myc mice [9]. Moreover, the bromodomain and extra-terminal (BET) family member, BRD4, modulates EZH2 transcription by upregulating MYC [10]. These observations highlight the critical role of EZH2 mutations and MYC overexpression in lymphomagenesis and the potential therapeutic benefit of targeting both factors to improve patient prognosis.

EZH2 genetic depletion or pharmacologic inhibition suppresses GC formation and functions, while somatic mutations reinforce these effects through enhanced silencing of EZH2 targets. Selective EZH2 inhibitors (EZH2i) are of significant interest, with the first-in-class tazemetostat showing a favorable safety profile and anti-tumor activity in refractory B-NHL [11]. However, results from a phase I/II trial (NCT01897571) in relapsed or refractory (R/R) DLBCL patients underscore the need for more potent and active compounds in this disease model. CPI169 (Constellation Pharmaceuticals), a structurally distinct and specific EZH2 inhibitor, was developed to enhance antitumor activity and effectively block the EZH2 epigenetic signature [12], demonstrating significant tumor regression in an EZH2-dependent tumor xenograft model [13]. Even though EZH2 inhibition shows limited clinical activity and may not be highly effective as a single agent, its combination with other drugs usually enhances therapeutical indexes [14,15].

To assess the suitability of combining EZH2 and MYC pharmacological inhibitors in B-NHL, we selected CPI203 (Constellation Pharmaceuticals), a preclinical formulation of the BRD4 antagonist CPI0610 (pelabresib). CPI203, developed from the first-in-class compound JQ1, harbors improved bioavailability in mice compared to its predecessor. Several preclinical studies have already confirmed CPI203′s MYC-dependent efficacy in DLBCL, mantle cell lymphoma (MCL), and multiple myeloma (MM), while highlighting the need for combination therapies to reach an optimal antitumor activity [16–18].

Although pharmacological targeting MYC and EZH2 may efficiently disrupt a MYC-miRNA-EZH2 oncogenic axis in aggressive B-cell lymphoma cells [6,8,19], *in* vivo validation and activity biomarkers for bench-to-bedside transfer are lacking. In the present work we evaluated the mechanisms of CPI169 antitumor activity alone and combined with the BRD4i CPI203 in EZH2^{Y641mut} and EZH2 ^{wt} DLBCL and FL cell lines, as well as an *in vivo* EZH2^{Y641mut} lymphoma model. We identified the upregulation of the mitosis regulator, YPEL2, and the consequent blockade of the cell cycle at G1 phase, as key drivers of the synergy between these two epigenetic drugs.

Materials and methods

Cell lines

Seven DLBCL (SUDHL-16, HT, SUDHL-4, Toledo, SUDHL-5, SUDHL-6, KARPAS-422) and two FL (WSU-FSCCL, RL) cell lines used in this study have been previously described [16,20]. Cells were grown in RPMI 1640 or DMEM, supplemented with 10 %−20 % heat-inactivated FBS, 2 mmol/L glutamine and 50 μg/mL penicillin-streptomycin (Thermo Fisher).

Generation of SUDHL-5 and HT EZH2 overexpressing cells and KARPAS-422 GFP$^+$Luc$^+$cells

To generate EZH2-coding retroviral particles, 3 × 10^6 Phoenix™ Ampho cells were transfected with 15 μg of FLAG-tagged EZH2^{Y641mut}, WT EZH2, or empty vector (EV) plasmids, (kindly provided by Dr. A. Melnick, Department of Medicine, Weill Cornell Medicine, New York, USA) [21] in the presence of X-tremeGENE HP DNA Transfection Reagent (Roche) according to the manufacturer's protocol. The viral supernatant was collected 48 h post-transfection, passed through a 0.45-μm filter, and used to infect 10^6 SUDHL-5 or HT cells in the presence of 4 μg/mL polybrene. Cells were spun in 24-well plates at 2.200 rpm for 2 h at 37 °C. Transduced cells were sorted based on GFP expression by using a FACSAria cell sorter (Becton-Dickinson).

To generate GFP-Luc-coding retroviral particles, 3 × 10^6 Phoenix™ Ampho cells were transfected with 15 μg of pMSCV-Luc2-PKG-Neo-IRES-GFP plasmid (Kindly provided by Dr. A. Zuber, Research Institute of Molecular Pathology (IMP), Vienna, Austria) in the presence of X-tremeGENE HP DNA Transfection Reagent (Roche) according to the manufacturer's protocol. The viral supernatant was collected 48 h post-transfection, passed through a 0.45 μm filter, and used to infect 10^6 KARPAS-422 cells in the presence of 4 μg/mL polybrene. Cells were spun in 24-well plates at 2.200 rpm for 2 h at 37 °C. Transduced cells were sorted based on GFP expression by using a FACSAria cell sorter (Becton-Dickinson).

Xenograft mouse model and tumor phenotyping

CB17-severe combined immunodeficiency (SCID) mice (Janvier labs, Le Genest-Saint-Isle, France) were inoculated subcutaneously with 10^7 KARPAS-422-GFP$^+$Luc$^+$ cells and monitored for tumor growth, bioluminescence signal, and vital parameters in compliance with the Animal Ethics Committee of the University of Barcelona (agreement #154/16) as previously described [16].

When tumors were palpable, mice were randomly assigned into cohorts of 4-5 animals each and received a BID injection of 1.25 mg/kg CPI203 (i.p.) and/or 50 mg/kg CPI169 (s.c.), or an equal volume of vehicle. After three weeks, animals were euthanized according to institutional guidelines and tumor samples were collected. Samples were snap-frozen in OCT medium (Sakura Tissue Tek, Alphen Aan den Rijn, Netherlands). RNA and protein analysis were performed by qPCR and western blot respectively ($n = 3$ mice per group).

Proliferation assay and cell cycle analysis

DLBCL and FL cells (4 × 10^4) were seeded on a 96-well plate and treated with 0.1-1 μM CPI169 for 7 days and/or 0.5-1 μM CPI203 from days 5-7 (kindly provided by Constellation Pharmaceuticals, Cambridge, MA, USA). Cell proliferation was determined by MTT (3-(4,5-dimethylthiazolyl-2)−2,5-diphenyltetrazolium bromide) method. Each measurement was performed in triplicate and values referred to untreated controls. Combination indexes (CIs) were calculated with Calcusyn software v2.0 (Biosoft, Ferguson, MO, USA), considering interactions significantly synergistic when CI < 0.8. For cell cycle analysis, treated cells were fixed overnight in 70 % ethanol, stained with propidium iodide (Sigma-Aldrich, Saint-Louis, MO, USA), and analyzed on a FACScalibur cytometer using Modfit v2.0 software (Becton-Dickinson, San Jose, CA, USA).

RNA interference assay

For transient down-regulation assays, KARPAS-422 and RL were electroporated using the Neon Transfection system (Thermo Fisher). To target *ABAT, KLHL14, PECI* and *YPEL2* genes, each targeted by 3 different small-interfering RNA (siRNA) sequences from TriFECTa Kit DsiRNA Duplex (Integrated DNA Technologies) were used for each target or a scrambled siRNA as a control. Briefly, cells were resuspended in 10 uL of buffer E with 1.5 μM of each siRNA pool. KARPAS-422 and RL were electroporated using 20 ms, 1 pulse and 1300 V or 1200 V respectively. Cells were seeded in 96-well plates, allowed to recover for 8 h post-transfection, and then treated with the compounds as described above. Proliferation was measured by MTT assay at day 3 post-transfection.

RNA isolation and real-time PCR

Total RNA was extracted using TRIZOL (Thermo Fisher) following

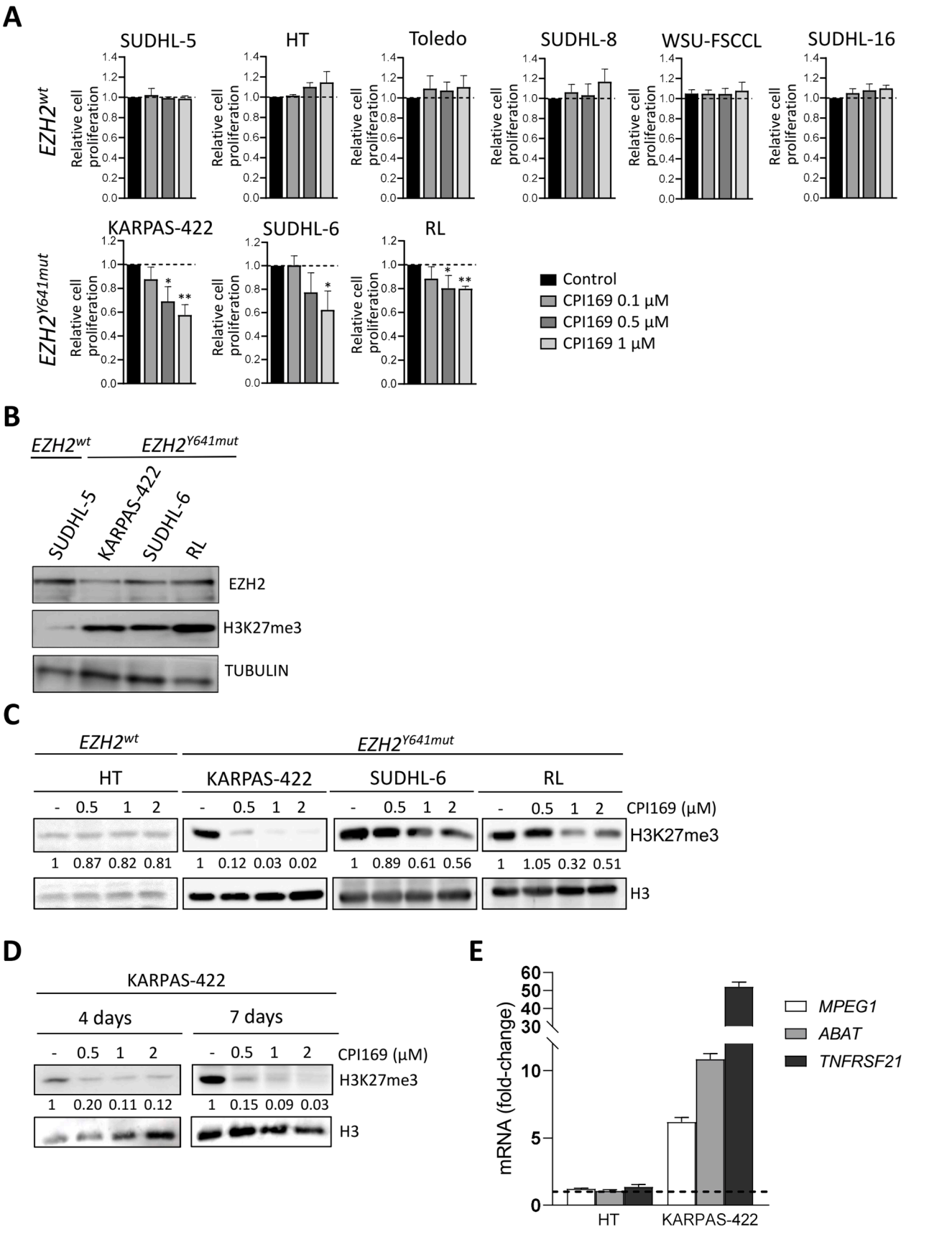

(caption on next page)

Fig. 1. CPI169 is active in EZH2^{Y641mut} cell lines of germinal center origin independently of EZH2 expression level and activity.
(A) MTT analysis in follicular lymphoma (FL) and diffuse large B cell lymphoma (DLBCL) cell lines treated with the indicated concentrations of CPI169 for 7 days and treatment was renewed at day 4. Data are expressed as mean ± SD of 3 replicates. (B) Western blot analysis of EZH2 and H3K27me3 in EZH2^{Y641mut} (KARPAS-422, SUDHL-6 and RL) and EZH2 ^{wt} (SUDHL5) cells. Tubulin was used as a loading control. (C) Western blot analysis of H3K27me in EZH2 ^{wt} (HT) and EZH2^{Y641mut} cells (SUDHL-6, RL, and KARPAS-422) treated with increasing doses of CPI169 for 4 days. H3 was used as a loading control. Values refer to the fold-change vs control (DMSO-treated) of the H3K27me3/H3 ratio. (D) Western blot analysis of H3K27me3 in KARPAS-422 treated with increasing doses of CPI169 for 4 and 7 days. H3 was used as a loading control. Values refer to the fold-change vs control (DMSO-treated) of the H3K27/H3 ratio. (E) qPCR analysis of *ABAT, MPEG1* and *TNFRSF21* mRNA levels in HT and KARPAS-422 cells treated with 1.5 μM CPI169 for 4 days. GAPDH was used as housekeeping gene. Values refer to the fold-change vs control (DMSO-treated) of the above-mentioned genes/GAPDH ratio. Comparisons are made between CPI169-treated vs. control (DMSO-treated) cells. Data are expressed as mean ± SD of 3 replicates. $^{*}P < 0.05$, $^{**}P < 0.01$, $^{***}P < 0.001$.

manufacturer's instructions. One microgram of RNA was retro-transcribed to complementary DNA using moloney murine leukemia virus reverse transcriptase (Thermo Fisher) and random hexamer primers (Roche). mRNA expression was analyzed in duplicate by quantitative real-time PCR on the Step one system by using predesigned Assay-on-Demand primers and probes (Thermo Fisher). The relative expression of each gene was quantified by the comparative cycle threshold method ($\Delta\Delta C_t$) (provided by request). β-actin, B2 M and or GAPDH were used as endogenous control.

Western blot

Total and nuclear extracts were obtained from 3 to 5 × 10^6 cells lysed on ice for 30 min in RIPA buffer (Sigma-Aldrich) supplemented with protease and phosphatase inhibitors. Lysates (30-50 μg) were separated on SDS-PAGE gels and proteins were transferred onto PVDF membranes (Immobilon-P, Merck-Millipore, Darmstadt, Germany). Membranes were incubated with primary and secondary antibodies (supplemental Table 3). Chemiluminescence detection was done using the ECL system (Pierce) and visualized on a mini-LAS4000 device using Image Gauge software (Fujifilm, Valhalla, NY, USA). Band intensity was quantified using Image J software and normalized to loading control protein (H3, GAPDH or Tubulin). Values were referred to the indicated control.

Gene expression and gene set enrichment (GSEA) analysis

DLBCL and FL cells (5 × 10^6) were seeded on a 6-well plate and treated with 1.5 μM CPI169 for 96 h and/or 0.5 μM CPI203 at 6 h prior to sample collection. Total RNA was then extracted as above and cRNA was hybridized on the HG-U219 GeneChip (Affymetrix, Santa Clara, CA, USA) following standardized protocols. Scanning was processed in a Gene Titan instrument and analyzed with GeneChip Command Console Software. Raw data were normalized using the Robust Multichip Analysis algorithm implemented in the Expression Console Software v1.1 (Affymetrix). Significant gene signatures differentially regulated by CPI169 ± CPI203 were identified with GSEA version 2.0 (Broad Institute at MIT; http://www.broadinstitute.org/gsea/) using the Hallmark gene sets, C2 (curated gene sets), C3 (motif gene sets), C5 (gene ontology gene sets) and C6 (oncogenic signatures) collections from the Molecular Signature Database v2.5, and custom gene sets (lymphochip.com). A two-class analysis with 1000 permutations of gene sets and a weighted metric was used. Gene sets with a false discovery rate (FDR) below 0.05 and a normalized enrichment score (NES) greater than 2 were considered significant. Expression heatmaps were generated using Morpheus software (Broad Institute at MIT; https://software.broadinstitute.org/morpheus/).

Statistical analysis

The presented data are the mean ± SD or SEM of 3 independent experiments. All statistical analyses were done by using GraphPad Prism 8.0 software (GraphPad Software). Comparison between 2 groups of samples was evaluated by nonparametric Mann–Whitney test to determine how response is affected by 2 factors. Pearson test was used to assess statistical significance of correlation. Results were considered statistically significant when p-value < 0.05.

Automated exploratory data analysis

To identify key genes associated with CPI169′s mechanism of action in FL/DLBCL cells, we conducted an automated exploratory data analysis (EDA) using AutoDiscovery 3.2 software (Butler Scientifics). AutoDiscovery is an automated, comprehensive EDA platform that enables systematic detection of relationships between variables while accounting for multiple testing and confounding factors, providing a framework for exploratory analyses. Experimental data on CPI169′s antitumoral effects, EZH2 mutation status, H3 methylation levels, and the top 200 genes up- or down-regulated in EZH2^{Y641mut} (but not EZH2 ^{wt}) cells (Threshold 13.5 %) were combined into a single dataset. AutoDiscovery systematically identified associations between variables using inferential statistical methods, including Spearman's Rank correlation coefficients, analysis of variances, and contingency analyses, selected automatically based on the data's nature and distribution. Given the high-dimensional nature of the data, AutoDiscovery incorporated multiple testing correction using the Benjamini-Hochberg false discovery rate (FDR) algorithm, classifying results as exploratory (p-value < 0.05) or confirmatory (p-value < FDR threshold, minimum threshold 0.02). The tool also addressed potential confounders through stratification to ensure robust association testing.

Results

CPI169 is active in mutated EZH2 cell lines of germinal center origin

To evaluate the sensitivity of GCB-DLBCL and FL cells to CPI169, a panel of six EZH2 ^{wt} and three EZH2^{Y641mut} cell lines was exposed to doses of CPI169 ranging from 0.1 to 1 μM, and proliferation was measured by MTT assay at 7 days. CPI169 exerted a dose-dependent cytotoxic activity in EZH2^{Y641mut} cells, reaching an average 35 % reduction (range: 20 - 48 %) in the relative number of proliferating cells at the 1 μM dose, while no effect was observed in EZH2 ^{wt} cell lines (Fig. 1A). Importantly, since its activity was restricted to EZH2^{Y641mut} cells, CPI169 antitumoral effect was not related to EZH2 protein basal levels in the tested cell lines, but rather to their basal methyltransferase activity, assessed by western blot detection of H3K27me3 histone mark (Fig. 1B). CPI169 led to a dose- and time-dependent reduction in H3K27me3 levels in EZH2^{Y641mut} cells (KARPAS-422, SUDHL-6 and RL), but not in the EZH2 ^{wt} cell line, HT (Figs 1C and D). Its activity was associated with the transcriptional upregulation of the known EZH2-repressed genes (*MPEG1, ABAT* and *TNFRSF21*[3]) specifically in EZH2^{Y641mut} cells (Fig. 1E).These data demonstrate the specific and significant antitumor activity of CPI169 in EZH2^{Y641mut} GC-derived cells.

Ectopic expression of EZH2Y641mut sensitizes DLBCL cells to CPI169

In order to identify a gene signature specifically associated with CPI169-mediated targeting of EZH2, cell lines with basal or ectopic expression of either EZH2^{Y641mut} or EZH2 ^{wt} were treated with CPI169 and analyzed. As shown in Fig. 2A, EZH2^{Y641mut} SUDHL-5 and HT

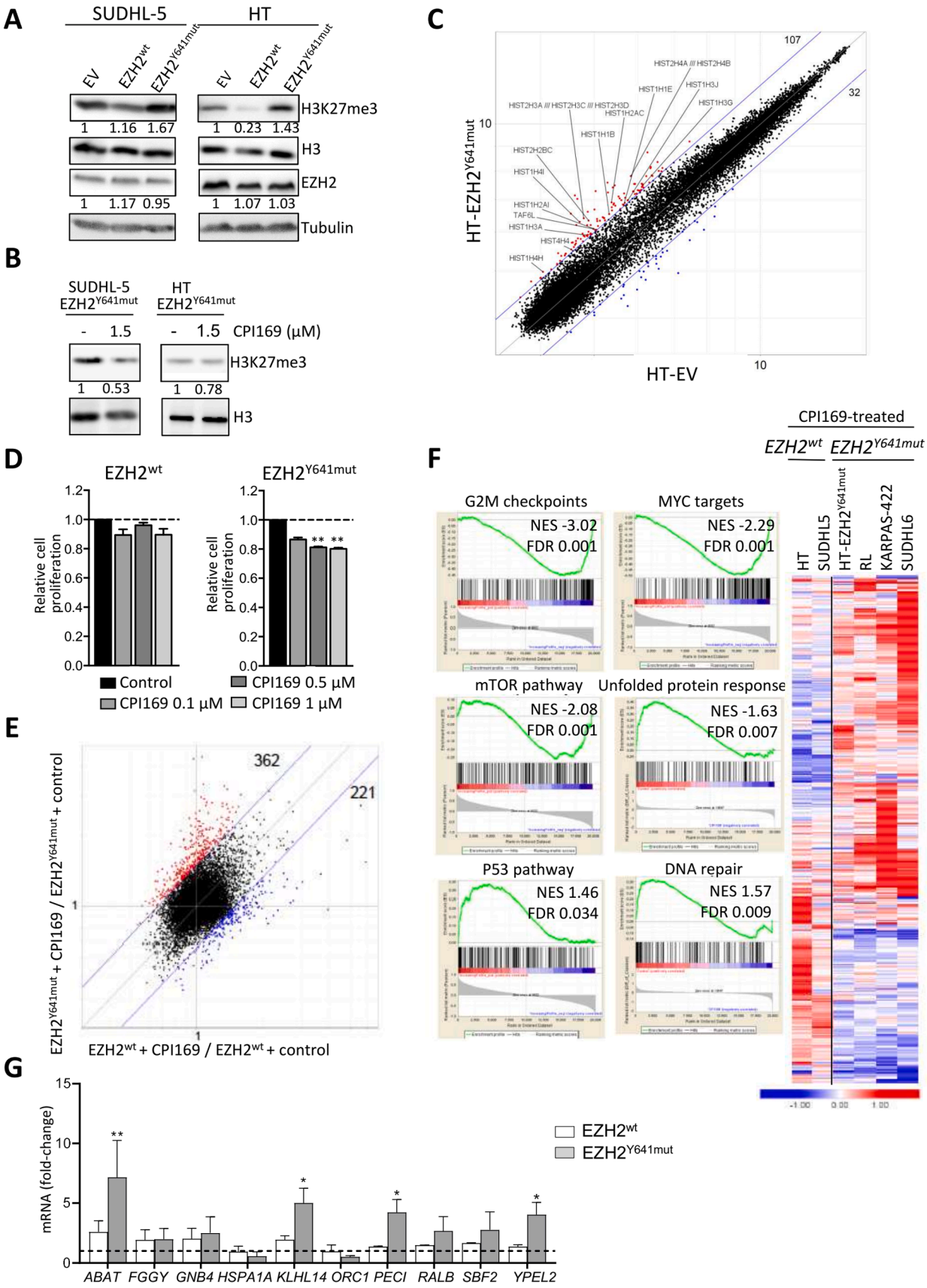

(caption on next page)

Fig. 2. EZH2 mutation at Y641 regulates cell sensitivity to CPI169.
(A) Western blot analysis of H3K27me3 and EZH2 from HT and SUDHL5 cells expressing FLAG-tagged EZH2^{Y641mut}, WT EZH2, or empty vector (EV). H3 and Tubulin was used as a loading control. Values refer to the fold-change vs control (EV) of the H3K27me3/H3 ratio or the EZH2/Tubulin ratio. (B) Western blot analysis of H3K27me3 from SUDHL5 and HT cells expressing FLAG-tagged EZH2^{Y641mut} or WT EZH2 and treated with 1.5 μM CPI169 for 4 days. H3 was used as a loading control. Values refer to the fold-change vs control (WT DMSO-treated) of the H3K27me3/H3 ratio. (C) Scatter plot from Gene Expression Profile (GEP) of HTEZ-H2^{Y641mut} vs HT-EV cells. (D) MTT analysis in SUDHL5 EZH2^{Y641mut} and SUDHL5 ^{wt} cells treated with the indicated concentrations of CPI169 for 7 days and renewed at day 4. Data are expressed as mean ± SD of 3 replicates. (E) GEP scatter plot from EZH2^{Y641mut} (KARPAS-422, SUDHL-6, RL, and HT EZH2^{Y641mut}) and EZH2 ^{wt} (HT and SUDHL5) cells treated with 1.5 μM CPI169 for 4 days. Red and blue dots represent up- and downregulated genes, respectively in EZH2^{Y641mut} cells. (F) Left panel: GSEA enrichment plots of mutated EZH2 signatures showing a correlation with sensitivity to CPI169. Right panel: heatmap showing genes differentially regulated upon CPI169 treatment in either EZH2 ^{wt} (HT, SUDHL5) or EZH2^{Y641mut} (RL, KARPAS-422, SUDHL6, and HT^{Y641N}) cell lines. (G) qPCR analysis of *ABAT, FGGY, GNB4, HSPA1A, KLHL14, ORC1, PECI, RALB, SBF2* and *YPEL2* mRNA levels in EZH2 ^{wt} (HT, SUDHL5) and EZH2^{Y641mut} (RL, KARPAS-422, SUDHL6) cells treated with 1.5 μM CPI169 for 4 days. β-actin/B2 M were used as housekeeping genes. Values refer to the fold-change vs control (DMSO-treated). Comparisons are made between CPI169-treated vs. control (DMSO-treated) cells. Data are expressed as mean ± SD of 3 replicates. *$P < 0.05$, **$P < 0.01$, ***$P < 0.001$.

subclones exhibited a 1.81-2.1-fold increase in basal H3K27me3 levels, compared to their EZH2 ^{wt} parental counterparts, with no significant modification of total EZH2 levels (Fig. 2A). Gene expression profiling of the HT subclones revealed that the expression of EZH2^{Y641mut} was linked to the upregulation of genes involved in chromatin organization (*HIST2H2BC, TAF6 L, HIST1H2AH*, and *HIST1H2AC*), when compared to empty vector (HT-EV) transfected cells (Fig. 2C). The consequent overall increase in methyltransferase activity rendered EZH2^{Y641mut} cells sensitive to CPI169, as illustrated by a downregulation of H3K27me3 levels in both EZH2^{Y641mut} cell lines cultured in the presence of the drug (Fig. 2B). This effect was associated with a slight, but significant 18-22 % increase in cell proliferation blockade (Fig. 2D).

To explore how EZH2 blockade achieves a superior antiproliferative effect in EZH2-mutated cells, FL and DLBCL cell lines with basal (RL, KARPAS-422, and SUDHL-6) or ectopic (HT-EZH2^{Y641mut}) expression of EZH2^{Y641mut} were treated with CPI169, and their gene expression profiles were compared to control (DMSO-treated) cells. As shown in Fig. 2E, we observed a differential whole gene modulation after CPI169 treatment in both cell subtypes, being 362 genes upregulated and 221 genes downregulated between EZH2^{Y641mut} and EZH2 ^{wt} cells (Supplemental Table 1). To determine the significance of these changes, we performed a GSEA [18], and found a significant downregulation of genes related to G2/M checkpoints, MYC targets, mTOR signaling, unfolded protein response, as well as up-regulation of genes related to P53 pathway and DNA repair, in EZH2^{Y641mut} exposed to CPI169, when compared to their EZH2 ^{wt} counterparts (Fig. 2F).

In order to identify the most relevant genes associated with the mechanism of action of CPI169 in FL and DLBCL cells, we underwent an automated and unbiased exploratory data analysis (EDA) (Supplemental Fig. 1A). For that aim, we carried out a correlation study between the main features of CPI169 activity, including antitumoral activity as assessed by MTT assay, cytofluorimetric determination of G1 cell cycle blockade, H3K27me3 histone mark loss quantification by western blot, and the top 200 genes most up- or downregulated upon EZHi therapy, specifically in mutated EZH2 cell lines (RL, KARPAS-422, and SUDHL-6) (Supplemental Table 1). Automated EDA analysis revealed a major effect of CPI169 treatment toward impairment of cell proliferation, over other mechanisms such as the expected regulation of chromatin organization [3,22] (Supplemental Fig. 1A). As shown in Supplemental Table 2, the expression of a reduced set of 10 genes was associated either positively (*ABAT, FGGY, GNB4, KLHL14, PECI, RALB, SBF2* and *YPEL2*) or negatively (*ORC1, HSPA1A*) to cell proliferation blockade in response to CPI169 treatment, exclusively in EZH2^{Y641mut} cells. Among these genes, only *ABAT, KLHL14, PECI* and *YPEL2* transcripts were confirmed to be significantly affected upon exposure to CPI169 in the whole set of EZH2^{Y641mut} cell lines, with no detectable modification in EZH2 ^{wt} cultures (Fig. 2G).

Altogether, these data suggest that the loss of H3K27me3 mark upon CPI169 treatment leads to the downregulation of mTOR, P53 and MYC signaling, triggering G1 cell cycle blockade, and that this phenomenon could be defined by a 4-gene signature (*ABAT, KLHL14, PECI* and *YPEL2)* specifically in EZH2^{Y641mut} lymphoma cells.

Bromodomain inhibition synergizes with CPI169 therapy in in vitro and in vivo models of DLBCL and FL with EZH2^{Y641mut}

Given the identification of MYC-regulated processes in the previous gene sets, and considering the relevant role of EZH2-MYC signaling axis in different types of aggressive B- and T-cell lymphomas [6,8,9,19,23] together with the limited clinical activity of EZH2i single-agent in B-NHL [14], we evaluated the potential combinational antitumor activity of MYC and EZH2 dual targeting in EZH2-mutated cells. To this end, we tested the effect of combining CPI169 with CPI203, a BRD4 inhibitor that disrupts the MYC transcriptional program in B-cell lymphoma [16,18,24], in a panel of EZH2^{Y641mut} and EZH2 ^{wt} cells. CPI203 treatment reduced MYC protein levels within 24 h, followed by EZH2 downregulation at 48 h, consistent with MYC's role in regulating EZH2 transcription [19] (Supplemental Fig. 1B). We then observed a synergistic antitumoral effect when cells were treated for 7 days with increasing doses of CPI169, and in combination with 0.1-0.5 μM CPI203 during the last 2 days, with combination indexes (CI) ranging from 0.062 to 0.904 (Fig. 3A, lower panels). In contrast, a barely additive or antagonistic drug interaction was observed in the EZH2 ^{wt} cell lines, with CIs higher than 1 (Fig. 3A, upper panel). To further address the mechanism underlying CPI203 and CPI169 cooperation in EZH2-mutated cell lines, we evaluated the impact of the drug combination on cell cycle progression. A 7-day sequential treatment with the two drugs increased the fraction of cells in the G0/G1 phase of the cell cycle up to 70 %−87 % and up to 76 %−87 % after exposure to single-agent CPI169 (1 μM) and CPI203 (0.5 μM), respectively. These values reached 83 %−91 % and 88 %−94 % according to the cell line, when the two drugs were used together. Of note, this drug combination failed to trigger a significant increase in apoptotic sub-G1 cell fraction, indicating that the efficacy of the doublet was mostly associated with an impairment of cell proliferation (Fig. 3B). We performed a gene expression profiling of KARPAS-422, SUDHL-6, RL, and HT- EZH2$^{Y641-mut}$ treated with 1.5 μM CPI169 for 96 h and/or with 0.5 μM CPI203 for 6 h prior to sample collection. The corresponding GSEA highlighted a synergistic downregulation of MYC-regulated genes in cells exposed to the drug combination. Most importantly, and in relation with the phenotype described above, two of the gene sets mostly affected by the drug combination corresponded to G2/M checkpoint regulators and to cell cycle and DNA replication, with a normalized enriched score (NES) of −2.08 and −2.378, respectively, and a false discovery rate (FDR) of 0 in both cases (Fig. 3C). These data confirmed a synergistic antiproliferative activity between CPI203 and CPI169, associated to MYC-EZH2 downregulation and regulation of cell cycle progression.

To confirm the efficacy CPI169/CPI203 combo in vivo, KARPAS-422-GFP+-Luc+ cells were inoculated subcutaneously into SCID mice and tumor-bearing mice were dosed with different treatment schedules. Monitoring of bioluminescence signal (Supplemental Fig. 1C) and calculation of tumor volume by external caliper (Fig. 3D) revealed that after 3 weeks of treatment, the combination-receiving arm showed the best response with a 62 % reduction of tumor volume when compared to baseline, and with 4 out of 5 (80 %) mice lacking detectable luciferase

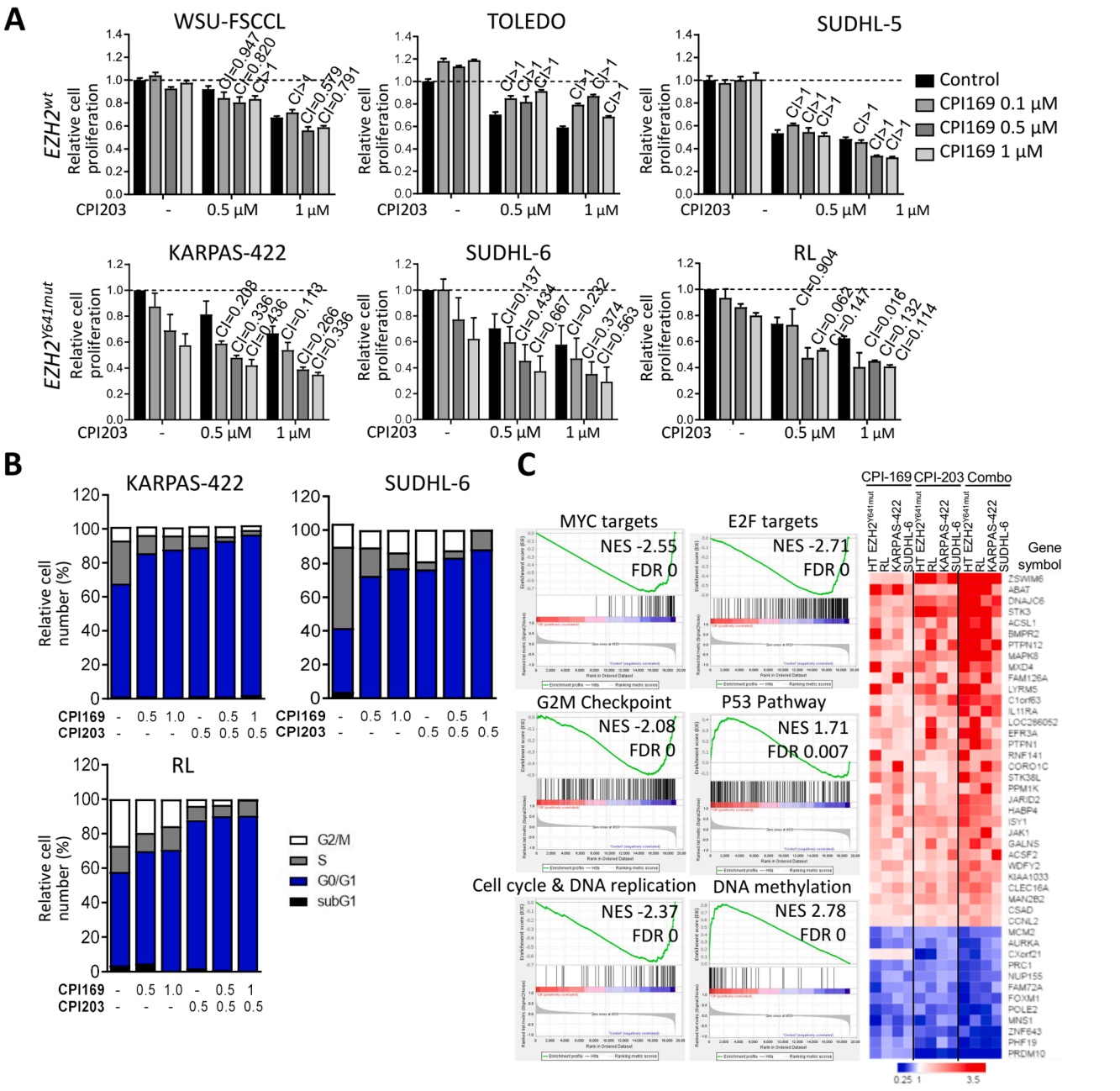

(caption on next page)

Fig. 3. The combination of CPI169 with the BET inhibitor CPI203 elicits a synergistic cell proliferation blockade in EZH2-mutated FL and DLBCL *in vitro* and *in vivo* models.
(A) MTT analysis in FL and DLBCL cell lines treated daily with the indicated concentrations of CPI169 for 7 days and 0.1 or 0.5 μM of CPI203 during the last 2 days. Combination indexes (CIs) were determined by the Chou and Talalay's algorithm (Calcusyn software). Combinational effect was considered significantly synergistic when CI < 0.8. Data are expressed as mean ± SD of 3 replicates. (B) Cell Cycle analysis of $EZH2^{Y641mut}$ cell lines treated with the indicated concentrations of CPI169 for 7 days and 0.1-0.5 μM of CPI203 for 2 days. (C) DLBCL and FL cells were treated with 1.5 μM CPI169 for 96 h and/or 0.5 μM CPI203 for 6 h prior to sample collection for gene expression profiling. Left panel: GSEA enrichment plots of the $EZH2^{Y641mut}$ signatures showing a correlation with sensitivity to CPI169 and CPI203. Right panel: heatmap showing a global enrichment in upregulated genes in $EZH2^{Y641mut}$ cells exposed to CPI169/CPI203 combo, when compared to single-agent therapies Top 45 up- and down-modulated genes are represented. (D) Recording of tumor volumes in the different treatment arms during the 3-week treatment, where means ± SEM are plotted. (E) Mean tumor weight at the day of sacrifice in the control ($n = 5$ animals) and the distinct drug treatment ($n = 6$ animals) groups. Comparisons are made between treated cells vs. control (DMSO-treated cells or vehicle-treated mice). Data are expressed as mean ± SD. $^{*}P < 0.05$, $^{**}P < 0.01$, $^{***}P < 0.001$.

activity. In comparison, although a lowest but persistent tumor regression was observed in the CPI169 group (−31 % vs baseline, consistent with the 37 % proliferation blockade achieved *in vitro*), the tumor activity remained detectable in all the animals. CPI203 single agent failed to evoke a deep tumor regression, despite achieving a noTable 80 % tumor growth inhibition when compared to vehicle. Conversely, tumor weight reduction reached 69 %, 59 % and 82 % in CPI169-, CPI203- and combo-receiving animals, respectively, when compared to vehicle-treated mice (Fig. 3E). In agreement with the *in vitro* results, the combination of CPI169/CPI203 was associated with a decrease in MYC expression and EZH2 activity, as assessed by WB (Supplemental Fig. 1D). Of note, no significant toxicity, as assessed by animal weight recording and vital parameters, was observed under the different treatment regimens (data not shown), thus suggesting that EZH2i-BETi dual treatment allows the control of $EZH2^{Y641mut}$ tumor growth with no remarkable adverse effects. This aspect is particularly relevant since prolonged therapy with bromodomain inhibitors has been associated with significant toxicity [25].

YPEL2 upregulation mediates the synergistic antitumor activity of CPI169 and CPI203 in $EZH2^{Y641mut}$ B-NHL models

To explore the relevance of the four genes previously identified by automated data analysis only in the CPI169 single-agent treatment and validated by qPCR, we used a siRNA approach to selectively downregulate the expression of *ABAT, KLHL14, PECI* and *YPEL2* in KARPAS-422 and RL prior to treatment with the different drugs and drug combinations as above. siRNA efficiency was confirmed in both cell lines by qPCR (Supplemental Fig. 1E). As shown in Fig. 4A, the four siRNA completely abrogated cell response to CPI169, whereas only the knockdowns of *YPEL2* and *KLHL14* significantly affected the activity of the CPI169/CPI203 combo in both RL and KARPAS-422 cells. Indeed, in KARPAS-422, the 65 % cytostatic effect observed upon treatment with the drug combination (see Fig. 3A), dropped down to 41 % and 45 % after *YPEL2* and *KLHL14* depletion, respectively. In RL cells, the activity of the combo was reduced down to 44 % after *YPEL2* interference, but was increased up to 76 % in the absence of *KHL14*, in both cases contrasting with the 59 % antitumor effect detected in normal conditions (see Fig. 3A). Thus, of the previously identified genes, only *YPEL2* transcriptional activation was required for full CPI169/CPI203 combinatorial activity in the two tested cell lines. Accordingly, we were unable to validate KLHL14 as a biomarker associated with CPI169/CPI203 combinational activity, as its regulation at mRNA or protein levels did not follow DLBCL and FL cell response to the drugs (Supplemental Fig. 1F and 1 G). Conversely, the expression of *YPEL2*, a PI3K/AKT-regulated gene and mitosis regulator [26], underwent a 1.4 to 3.3-fold and a 1.3 to 2.1-fold increase in mRNA and protein levels, respectively, in RL and KARPAS-422 cells treated with CPI169 single agent *in vitro* (Fig. 4B and C). We further observed that in cells exposed to the combination treatment, YPEL2 mRNA and protein levels underwent a 1.7-3.4 fold and a 2.4-5.1-fold increase, respectively. This accumulation of YPEL2 in the combination of CPI169/CPI203 was also confirmed in the tumors *in vivo*, both by western blot and qPCR with a 5.3 and a 41-fold increase, respectively (Fig. 4D and E).

In line with its role as a negative regulator of mitotic assembly [27,28], *YPEL2* silencing was associated with a remarkable downregulation of the cell cycle inhibitors P21/CDKN1A and GADD45A, and with the intracellular accumulation of the mitotic marker, histone H3-pSer10, at mRNA and/or protein levels (Figs. 4F and G). Of note, when compared to single-agent treatments, the accumulation of both *GADD45A* and *CDKN1A* mRNA was enhanced in cultures subjected to CPI169/CPI203 combination *in vitro* (Fig. 4C and Supplemental Fig. 1H) and confirmed in *in vivo* tumor specimens (Fig. 4E). These data strongly suggest that the transcriptional upregulation of *YPEL2* is required for the synergistic dual targeting of MYC/EZH2 in $EZH2^{Y641mut}$ B-NHL models.

Discussion

EZH2 point mutations are considered early clonal events in lymphomagenesis and are maintained through disease progression [29]. Gain-of-function mutations and/or overexpression of EZH2 arrest B lymphocytes in a state of immaturity and perpetual proliferation. Over the past decade, efforts to develop selective EZH2 inhibitors have highlighted CPI169 as an effective treatment [30]. Here, we demonstrated that CPI169 exerts a significant antitumoral effect and selectively suppressed H3K27me3 in DLBCL and FL $EZH2^{Y641mut}$cells, consistent with previous studies showing superior efficacy of EZH2 inhibitors in EZH2 GC-derived lymphoma mutated cell lines [3,31,32].

In this study, we identify a gene signature associated with $EZH2^{Y641mut}$ expressing cell response to selective inhibition of the methyltransferase. EDA revealed a major effect of CPI169 treatment on impairment of cell proliferation, over other mechanisms, such as chromatin organization, as previously described in other studies using different EZH2 inhibitors [3,22]. This approach allowed us to identify a limited set of 5 genes that were specifically associated with EZH2 disruption in mutated, but not wild-type cells, which may account for the superior activity of EZH2is in the first group of cells [8,19,23,33].

The relationship between the gene sets mostly affected by CPI169 treatment, and the central role of MYC-EZH2 oncogenic axis or loop in different types of aggressive B cell or T cell lymphomas led us to evaluate whether the dual-targeting of MYC and EZH2 might exert combinational antitumoral activity in EZH2-mutated cells. Our combination analysis confirmed a synergistic activity between the BETi, CPI203, and CPI169, in terms of proliferation blockade, MYC-EZH2 downregulation, and the regulation of cell cycle checkpoints. Mechanistically, it is plausible to assume that MYC represses EZH2 through induction of the EZH2-targeting miRNAs, such as miR-26a, miR26b and miR-101 [6,8,19]. This interaction could underline the cooperative relationship between both agents. *In vitro* studies on dual-targeting of MYC and EZH2, using JQ1 and DZNep compounds, have demonstrated the potential to disrupt the oncogenic MYC-EZH2 axis in aggressive B-cell lymphoma by suppressing MYC expression, promoting lymphoma cell death and inhibiting clonogenic growth [8]. However, the safety and efficacy of this approach in animal models of human lymphoma have not yet been investigated. No drug efficacy biomarkers have been identified for this dual strategy in B-cell lymphoma, though combining EZH2 and BET

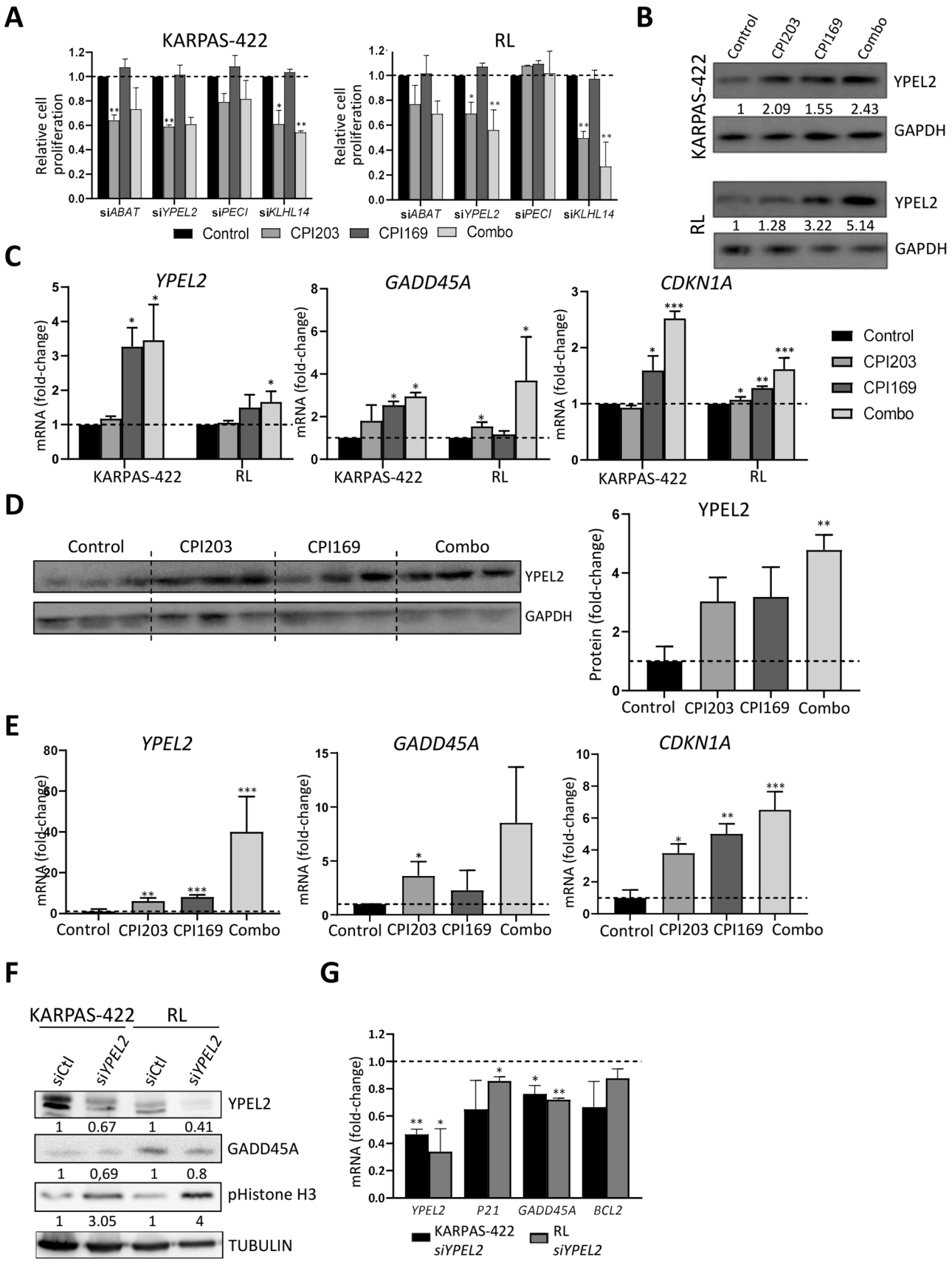

(caption on next page)

Fig. 4. YPEL2 upregulation is required for the synergistic antitumor activity of CPI169 and CPI203 in $EZH2^{Y641mut}$ B-NHL.
(A) siRNA screening of *ABAT, KLHL14, PECI,* and *YPEL2* in KARPAS-422 and RL cells exposed to CPI169 (1.5 μM), CPI203 (0.5 μM) or the drug combination for 72 h, as assessed by MTT assay. Data are expressed as fold change vs control (scramble siRNA, not treated, siCtl, $n = 3$ biological replicates). (B) Western blot analysis of YPEL2 and (C) qPCR determination of *YPEL2, GADD45A* and *CDKN1A* mRNA levels in KARPAS-422 and RL cells treated by 1.5 μM CPI169 for 96 h and/or 0.5 μM CPI203 for 48 h. GAPDH was used as a loading control. Values are referred to control untreated cells. (D) Western blot analysis of YPEL2 in representative tumor samples ($N = 3$ tumors per group). GAPDH was used as a loading control. *Right panel*: densitometric quantification of the YPEL2/GAPDH ratio. Values are referred to control (vehicle-treated) tumors. (E) qPCR analysis of *YPEL2, GADD45A*, and *CDKN1A* mRNA levels in representative tumor samples ($n = 3$ tumors per group). GAPDH was used as a housekeeping gene. Values are referred to control (vehicle-treated) tumors. (F) Western blot and (G) qPCR analyses of YPEL2 and cell cycle-related markers in KARPAS-422 and RL cell lines electroporated with either si*YPEL2* or siCtl for 8 h. Tubulin and β-actin/B2 M were used as loading control and housekeeping gene, respectively. Values are referred to control (siCtl-transfected) cells. Data are expressed as mean ± SD of 3 replicates. $^{*}P < 0.05$, $^{**}P < 0.01$, $^{***}P < 0.001$.

inhibitors has shown potential to inhibit proliferation and induce apoptosis via epigenetic regulation of tumor suppressors in diffuse intrinsic pontine glioma [34]. Here we provide evidence that EZH2i-BETi dual treatment is feasible and allows a remarkable control of tumor growth, achieving an almost complete tumor regression after a 3-week treatment, with no notable toxicity, in $EZH2^{mut}$ tumor-bearing animals. This is particularly encouraging, as prolonged therapy with bromodomain inhibitors is often associated with significant toxicities. Specifically, these agents may cause up to a 50 % reduction in platelet counts in rodents after 14 days of daily administration. [35,36] In contrast, our findings show that BID administration of CPI203, in combination therapy over 3 weeks, does not exhibit such systemic toxicity. However, long-term studies are needed to confirm these results and provide a more thorough evaluation of the safety profile of the BETi-EZH2i combination. In addition, potential resistance mechanisms to these agents must be carefully considered. In DLBCL, resistance to EZH2 inhibitors has been attributed to the activation of compensatory pathways such as IGF-1R, PI3 K, and MEK, which counteract the therapeutic effects of EZH2 inhibition [37,38]. Similarly, resistance to BRD4 inhibitors often arises through mechanisms that restore MYC expression following prolonged exposure to bromodomain inhibitors [39]. By simultaneously targeting both EZH2 and BRD4, this dual-therapy approach may mitigate compensatory pathway activation and delay resistance, potentially leading to a more durable therapeutic response. Future research should investigate the dynamics of resistance during long-term treatments and assess whether incorporating inhibitors of IGF-1R, PI3 K, or MEK pathways could further enhance the efficacy of this combinatorial strategy.

In addition, by both *in vitro* siRNA screening of the selected genes and *in vivo* phenotypic analysis, we found that those effects were related to the abrogation of MYC transcriptional program and a lowering of tumor mitotic index, involving two potent biomarkers of drug efficacy, KLHL14 and YPEL2. Among the genes initially analyzed, only YPEL2 demonstrated consistent activation in response to CPI169 and to the CPI169/CPI203 combination. Notably, the combinatorial treatment elicited a pronounced increase in YPEL2 expression both in vitro and in vivo, underscoring its potential as a therapeutic biomarker of response in $EZH2^{Y641mut}$ B-NHL. By contrast, KLHL14, which was associated with drug response, failed to exhibit regulation correlating with drug activity, suggesting that its role in this context is limited.

Supporting the notion that high levels of YPEL2 are associated with lower tumor burden, B-cell lymphoma patients harboring higher expression of YPEL2 present a better prognosis (Supplemental Fig. 1I). While these findings provide initial evidence supporting the potential role of YPEL2 as a prognostic marker of response to determined epigenetic drugs in DLBCL and FL, future studies with large sets of fully annotated patient-derived samples and xenograft models, will be necessary to confirm these results.

Collectively, our results demonstrate that the combined inhibition of bromodomain protein and EZH2 is safe and efficacious in both *in vitro* and *in vivo* models of B-NHL, and that it can be monitored by a specific biomarker, YPEL2, and a proliferation gene signatures, reflecting the crucial role of $EZH2^{Y641mut}$ signaling in the control of cell proliferation of tumors of germinal center origin.

CRediT authorship contribution statement

Aránzazu Chamorro-Jorganes: Writing – original draft, Validation, Methodology, Investigation, Conceptualization. **Núria Profitós-Pelejà:** Writing – original draft, Validation, Methodology, Investigation, Formal analysis, Conceptualization. **Clara Recasens-Zorzo:** Methodology, Investigation. **Juan G Valero:** Methodology, Investigation. **Diana Reyes-Garau:** Methodology, Investigation. **Laura Magnano:** Validation. **Ray Butler:** Software. **Antonio Postigo:** Validation, Funding acquisition. **Patricia Pérez-Galán:** Writing – review & editing, Validation. **Marcelo Lima Ribeiro:** Writing – original draft, Validation, Supervision, Conceptualization. **Gaël Roué:** Writing – review & editing, Writing – original draft, Validation, Supervision, Project administration, Investigation, Funding acquisition, Formal analysis, Conceptualization.

Declaration of competing interest

The authors declare the following financial interests/personal relationships which may be considered as potential competing interests:

G. Roué received research funding from TG Therapeutics, Inc. and Kancera AB, to support studies unrelated to the present work. The remaining authors have no competing financial interests.

Acknowledgements

The authors thank Dr Ari Melnick (Weill Cornell Medicine, New York, USA) for providing the EZH2 plasmids and Vanina Rodríguez (IDIBAPS, Barcelona, Spain) for expert technical assistance. CPI203 and CPI169 were kindly provided by Constellation Pharmaceuticals, Inc. This work was financially supported by Fondo de Investigación Sanitaria PI15/00102 and PI18/01383, European Regional Development Fund (ERDF) 'Una manera de hacer Europa' (to G.R.) and the Spanish National Research Agency (AEI-MICINN) (SAF2017-84918-R and PID2020-116338RB-I00) to A.P. A.C.-J. hold a postdoctoral fellowship from the Agency for Management of University and Research (AGAUR, Beatriu de Pinós 2014 BP-B00177). C.R.-Z. was recipient of a predoctoral fellowship from Instituto de Salud Carlos III (grant PIE13/00033). The authors thank CERCA Programme/Generalitat de Catalunya for institutional support.

Supplementary materials

Supplementary material associated with this article can be found, in the online version, at doi:10.1016/j.neo.2025.101131.

References

[1] T. Chen, S.Y.R. Dent, Chromatin modifiers and remodellers: regulators of cellular differentiation, Nat. Rev. Genet. 15 (2014) 93–106.
[2] R.D. Morin, N.A. Johnson, T.M. Severson, A.J. Mungall, J. An, R. Goya, et al., Somatic mutations altering EZH2 (Tyr641) in follicular and diffuse large B-cell lymphomas of germinal-center origin, Nat. Genet. 42 (2010) 181–185.
[3] M.T. McCabe, H.M. Ott, G. Ganji, S. Korenchuk, C. Thompson, G.S. Van Aller, et al., EZH2 inhibition as a therapeutic strategy for lymphoma with EZH2-activating mutations, Nature 492 (2012) 108–112.

[4] J.C. van Galen, D.F. Dukers, C. Giroth, R.G.A.B. Sewalt, A.P. Otte, C.J.L.M. Meijer, et al., Distinct expression patterns of polycomb oncoproteins and their binding partners during the germinal center reaction, Eur. J. Immunol. 34 (2004) 1870–1881.

[5] I. Velichutina, R. Shaknovich, H. Geng, N.A. Johnson, R.D. Gascoyne, A. M. Melnick, et al., EZH2-mediated epigenetic silencing in germinal center B cells contributes to proliferation and lymphomagenesis, Blood 116 (2010) 5247–5255.

[6] X. Zhang, X. Zhao, W. Fiskus, J. Lin, T. Lwin, R. Rao, et al., Coordinated silencing of MYC-mediated miR-29 by HDAC3 and EZH2 as a therapeutic target of histone modification in aggressive B-cell lymphomas, Cancer Cell 22 (2012) 506–523.

[7] R.J.H. Ryan, M. Nitta, D. Borger, L.R. Zukerberg, J.A. Ferry, N.L. Harris, et al., EZH2 Codon 641 mutations are common in BCL2-rearranged germinal center B cell lymphomas, PLoS. One 6 (2011), https://doi.org/10.1371/journal.pone.0028585.

[8] X. Zhao, T. Lwin, X. Zhang, A. Huang, J. Wang, V.E. Marquez, et al., Disruption of the MYC-miRNA-EZH2 loop to suppress aggressive B-cell lymphoma survival and clonogenicity, Leukemia 27 (2013) 2341–2350.

[9] T. Berg, S. Thoene, D. Yap, T. Wee, N. Schoeler, P. Rosten, et al., A transgenic mouse model demonstrating the oncogenic role of mutations in the polycomb-group gene EZH2 in lymphomagenesis, Blood 123 (2014) 3914–3924.

[10] X. Wu, D. Liu, D. Tao, W. Xiang, X. Xiao, M. Wang, et al., BRD4 regulates EZH2 transcription through upregulation of C-MYC and represents a novel therapeutic target in bladder cancer, Mol. Cancer Ther. 15 (2016) 1029–1042.

[11] A. Italiano, J.C. Soria, M. Toulmonde, J.M. Michot, C. Lucchesi, A. Varga, et al., Tazemetostat, an EZH2 inhibitor, in relapsed or refractory B-cell non-hodgkin lymphoma and advanced solid tumours: a first-in-human, open-label, phase 1 study, Lancet Oncol. 19 (2018) 649–659.

[12] S. Garapaty-Rao, C. Nasveschuk, A. Gagnon, E.Y. Chan, P. Sandy, J. Busby, et al., Identification of EZH2 and EZH1 small molecule inhibitors with selective impact on diffuse large B cell lymphoma cell growth, Chem. Biol. 20 (2013) 1329–1339.

[13] V.S. Gehling, R.G. Vaswani, C.G. Nasveschuk, M. Duplessis, P. Iyer, S. Balasubramanian, et al., Discovery, design, and synthesis of indole-based EZH2 inhibitors, Bioorganic Med. Chem. Lett. 25 (2015) 3644–3649.

[14] M. Fernández-Serrano, R. Winkler, J.C. Santos, Pannérer M-M Le, M. Buschbeck, G Roué, Histone modifications and their targeting in lymphoid malignancies, Int. J. Mol. Sci. 23 (2021) 253. *2022, Vol 23, Page 253*.

[15] M.L. Eich, M. Athar, J.E. Ferguson, S. Varambally, EZH2-targeted therapies in cancer: hype or a reality, Cancer Res. 80 (2020) 5449–5458.

[16] C. Recasens-Zorzo, T. Cardesa-Salzmann, P. Petazzi, L. Ros-Blanco, A. Esteve-Arenys, G. Clot, et al., Pharmacological modulation of CXCR4 cooperates with BET bromodomain inhibition in diffuse large B-cell lymphoma, Haematologica 104 (2018) haematol.2017.180505.

[17] T. Díaz, V. Rodríguez, E. Lozano, M.P. Mena, M. Calderón, L. Rosiñol, et al., The BET bromodomain inhibitor CPI203 improves lenalidomide and dexamethasone activity in in vitro and in vivo models of multiple myeloma by blockade of ikaros and MYC signaling, Haematologica 102 (2017) 1776–1784.

[18] A. Moros, V. Rodríguez, I. Saborit-Villarroya, A. Montraveta, P. Balsas, P. Sandy, et al., Synergistic antitumor activity of lenalidomide with the BET bromodomain inhibitor CPI203 in bortezomib-resistant mantle cell lymphoma, Leukemia 28 (2014) 2049–2059.

[19] S. Sander, L. Bullinger, K. Klapproth, K. Fiedler, H.A. Kestler, T.F.E. Barth, et al., MYC stimulates EZH2 expression by repression of its negative regulator miR-26a, Blood 112 (2008) 4202–4212.

[20] A. Matas-Céspedes, V. Rodriguez, S.G. Kalko, A. Vidal-Crespo, L. Rosich, T. Casserras, et al., Disruption of follicular dendritic cells-follicular lymphoma cross-talk by the pan-PI3K inhibitor BKM120 (buparlisib), Clin. Cancer Res. 20 (2014) 3458–3471.

[21] W. Béguelin, R. Popovic, M. Teater, Y. Jiang, K.L. Bunting, M. Rosen, et al., EZH2 Is required for germinal center formation and somatic EZH2 mutations promote lymphoid transformation, Cancer Cell 23 (2013) 677–692.

[22] W. Qi, H.M. Chan, L. Teng, L. Li, S. Chuai, R. Zhang, et al., Selective inhibition of Ezh2 by a small molecule inhibitor blocks tumor cells proliferation, Proc. Natl. Acad. Sci. U S A 109 (2012) 21360–21365.

[23] J. Yan, S.B. Ng, J.L.S. Tay, B. Lin, T.L. Koh, J. Tan, et al., EZH2 overexpression in natural killer/T-cell lymphoma confers growth advantage independently of histone methyltransferase activity, Blood 121 (2013) 4512–4520.

[24] I. Dlouhy, M. Armengol, C. Recasens-Zorzo, M.L. Ribeiro, P. Pérez-Galán, F. Bosch, et al., Interleukin-1 receptor associated kinase 1/4 and bromodomain and extra-terminal inhibitions converge on NF-κb blockade and display synergistic antitumoral activity in activated B-cell subset of diffuse large B-cell lymphoma with MYD88 L265P mutation, Haematologica 106 (2021) 2749.

[25] M.L. Ribeiro, D. Reyes-Garau, M. Armengol, M. Fernández-Serrano, G. Roué, Recent advances in the targeting of epigenetic regulators in b-cell non-hodgkin lymphoma, Front. Genet. 10 (2019), https://doi.org/10.3389/fgene.2019.00986.

[26] O. Delpuech, C. Rooney, L. Mooney, D. Baker, R. Shaw, M. Dymond, et al., Identification of pharmacodynamic transcript biomarkers in response to FGFR inhibition by AZD4547, Mol. Cancer Ther. 15 (2016) 2802–2813.

[27] N. Han, F. Yuan, P. Xian, N. Liu, J. Liu, H.H. Zhang, et al., GADD45a mediated cell cycle inhibition is regulated by p53 in bladder cancer, Onco. Targets. Ther. 12 (2019) 7591–7599.

[28] H. Zhao, S. Jin, M.J. Antinore, F.D.T. Lung, F. Fan, P. Blanck, et al., The central region of Gadd45 is required for its interaction with p21/WAF1, Exp. Cell Res. 258 (2000) 92–100.

[29] C. Bödör, V. Grossmann, N. Popov, J. Okosun, C. O'Riain, K. Tan, et al., EZH2 mutations are frequent and represent an early event in follicular lymphoma, Blood 122 (2013) 3165–3168.

[30] R.G. Vaswani, V.S. Gehling, L.A. Dakin, A.S. Cook, C.G. Nasveschuk, M. Duplessis, et al., Identification of (R)-N-((4-Methoxy-6-methyl-2-oxo-1,2-dihydropyridin-3-yl) methyl)-2-methyl-1-(1-(1-(2,2,2-trifluoroethyl)piperidin-4-yl)ethyl)-1H-indole-3-carboxamide (CPI-1205), a potent and selective inhibitor of histone methyltransferase EZH2, suitable for Phase i clinical trials for B-cell lymphomas, J. Med. Chem. 59 (2016) 9928–9941.

[31] S.K. Knutson, S. Kawano, Y. Minoshima, N.M. Warholic, K.C. Huang, Y. Xiao, et al., Selective inhibition of EZH2 by EPZ-6438 leads to potent antitumor activity in EZH2-mutant non-hodgkin lymphoma, Mol. Cancer Ther. 13 (2014) 842–854.

[32] M.T. McCabe, A.P. Graves, G. Ganji, E. Diaz, W.S. Halsey, Y. Jiang, et al., Mutation of A677 in histone methyltransferase EZH2 in human B-cell lymphoma promotes hypertrimethylation of histone H3 on lysine 27 (H3K27), Proc. Natl. Acad. Sci. U S A 109 (2012) 2989–2994.

[33] S. Zhang, D.G. Konstantinidis, J.Q. Yang, B. Mizukawa, K. Kalim, R.A. Lang, et al., Gene targeting RhoA reveals its essential role in coordinating mitochondrial function and thymocyte development, J. Immunol. 193 (2014) 5973–5982.

[34] Y. Zhang, W. Dong, J. Zhu, L. Wang, X. Wu, H. Shan, Combination of EZH2 inhibitor and BET inhibitor for treatment of diffuse intrinsic pontine glioma, Cell Biosci. 7 (2017), https://doi.org/10.1186/s13578-017-0184-0.

[35] S. Bhattacharya, S. Piya, G. Borthakur, Bromodomain inhibitors: what does the future hold? Clin. Adv. Hematol. Oncol. 16 (2018).

[36] M.M. Mita, A.C. Mita, Bromodomain inhibitors a decade later: a promise unfulfilled? Br. J. Cancer 123 (2020) 1713–1714. *2020 12312*.

[37] M. Bisserier, N.W. Blood, Mechanisms of resistance to EZH2 inhibitors in diffuse large B-cell lymphomas. *Ashpublications.Org M Bisserier, N WajapeyeeBlood*, J. Am. Soc. Hematol. (2018) *ashpublications.org*, https://ashpublications.org/blood/article-abstract/131/19/2125/36914 (accessed 13 Jan2025).

[38] T. Baker, S. Nerle, J. Pritchard, B. Zhao, V.M. Rivera, A. Garner, et al., Acquisition of a single EZH2 D1 domain mutation confers acquired resistance to EZH2-targeted inhibitors, Oncotarget. 6 (2025). www.impactjournals.com/oncotarget/ (accessed 13 Jan).

[39] J. Calder, A. Nagelberg, J. Luu, D. Lu, W.W. Lockwood, Resistance to BET inhibitors in lung adenocarcinoma is mediated by casein kinase phosphorylation of BRD4, Oncog 10 (2021) 1–15. *2021 103*.